powerful technique for the low-energy range ($\lesssim 0.1$ eV). On the other hand, inelastic X-ray scattering is well suited for the study of high momentum and large energy transfers because the energy resolution is limited to ~ 1 eV and the cross section increases with momentum transfer. In the intermediate range, inelastic electron scattering [or electron energy-loss spectroscopy (EELS)] is the most useful technique. For recent reviews on different aspects of the subject, the reader may consult the texts by Schnatterly (1979), Raether (1980), Colliex (1984), Egerton (1986), and Spence (1988).

4.3.4.1.2. *Parameters involved in the description of a single inelastic scattering event*

The importance of inelastic scattering as a function of energy and momentum transfer is governed by a double differential cross section:

$$\frac{\mathrm{d}^2\sigma}{\mathrm{d}\Omega\,\mathrm{d}(\Delta E)}, \tag{4.3.4.1}$$

where $\mathrm{d}\Omega$ corresponds to the solid angle of acceptance of the detector and $\mathrm{d}(\Delta E)$ to the energy window transmitted by the spectrometer. The experimental conditions must therefore be defined before any interpretation of the data is possible. Integrations of the cross section over the relevant angular and energy-loss domains correspond to partial or total cross sections, depending on the feature measured. For instance, the total inelastic cross section (σ_i) corresponds to the probability of suffering any energy loss while being scattered into all solid angles. The discrimination between elastic and inelastic signal is generally defined by the energy resolution of the spectrometer, that is the minimum energy loss that can be unambiguously distinguished from the zero-loss peak; it is therefore very dependent on the instrumentation used.

The kinematics of a single inelastic event can be described as shown in Fig. 4.3.4.2. In contrast to the elastic case, there is no simple relation between the scattering angle θ and the transfer of momentum $\hbar\mathbf{q}$. One has also to take into account the energy loss ΔE. Combining both equations of conservation of momentum and energy,

$$\frac{\hbar^2 k'^2}{2m_0} + \Delta E = \frac{\hbar^2 k^2}{2m_0}, \tag{4.3.4.2}$$

and

$$q^2 = k^2 + k'^2 - 2kk'\cos\theta, \tag{4.3.4.3}$$

one obtains

$$(qa_0)^2 = \frac{2E_0}{R}\left[1 - \left(1 - \frac{\Delta E}{E_0}\right)^{1/2}\cos\theta\right] - \frac{\Delta E}{R}, \tag{4.3.4.4}$$

where the fundamental units $a_0 = \hbar^2/m_0e^2 =$ Bohr radius and $R = m_0e^4/2\hbar^2 =$ Rydberg energy are used to introduce dimensionless quantities. In this kinematical description, one deals only with factors concerning the primary or the scattered particle, without considering specifically the information on the ejected electron. For a core-electron excitation of an atom, one distinguishes $\mathbf{q}$ (the momentum exchanged by the incident particle) and $\boldsymbol{\chi}$ (the momentum gained by the excited electron), the difference being absorbed by the recoil of the target nucleus (Maslen & Rossouw, 1983).

4.3.4.1.3. *Problems associated with multiple scattering*

The strong coupling potential between the primary electron and the solid target is responsible for the occurrence of multiple inelastic events (and of mixed inelastic–elastic events) for thick specimens. To describe the interaction of a primary particle with an assembly of randomly distributed scattering centres (with a density N per unit volume), a useful concept is the mean free path defined as

$$\Lambda = 1/N\sigma \tag{4.3.4.5}$$

for the cross section σ. The ratio t/Λ measures the probability of occurrence of the event associated with the cross section σ when the incident particle travels a given length t through the material. This is true in the single scattering case, that is when $t/\Lambda \ll 1$.

For increased thicknesses, one must take into account all multiple scattering events and this contribution begins to be non-negligible for $t \gtrsim$ a few tens of nanometres. Multiple scattering is responsible for a broadening of the angular distribution of the

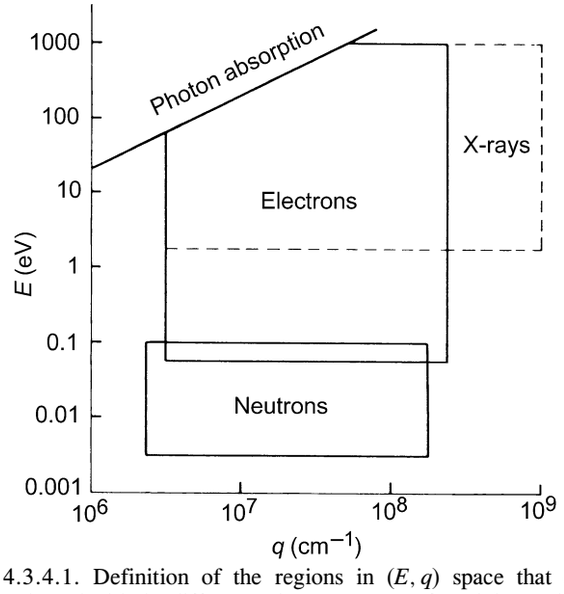

Fig. 4.3.4.1. Definition of the regions in (E, q) space that can be investigated with the different primary sources of particles available at present [courtesy of Schnatterly (1979)].

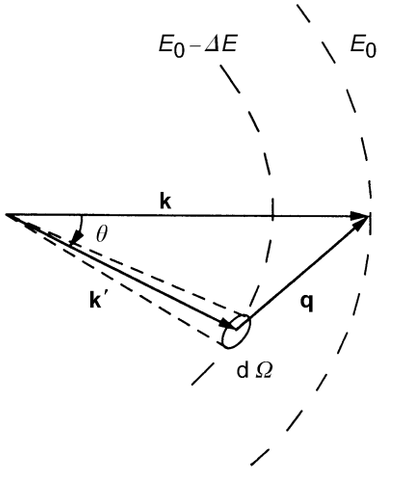

Fig. 4.3.4.2. A primary electron of energy E_0 and wavevector $\mathbf{k}$ is inelastically scattered into a state of energy $E_0 - \Delta E$ and wavevector $\mathbf{k}'$. The energy loss is ΔE and the momentum change is $\hbar\mathbf{q}$. The scattering angle is θ and the scattered electron is collected within an aperture of solid angle $\mathrm{d}\Omega$.

scattering electrons – mostly due to single or multiple elastic events – and of an important fraction of inelastic electrons suffering more than one energy loss. The probability of having n inelastic processes of mean free path Λ is governed by the Poisson distribution:

$$P_n(t) = \frac{1}{n!}\left(\frac{t}{\Lambda}\right)^{-n} \exp\left(-\frac{t}{\Lambda}\right). \qquad (4.3.4.6)$$

Multiple losses introduce additional peaks in the energy-loss spectrum; they are also responsible for an increased background that complicates the detection of single characteristic core-loss signals. Consequently, when the specimen thickness is not very small (*i.e.* for $t \gtrsim 50$ nm for 100 keV primary electrons), it is necessary to retrieve the single scattering profile that is truly representative of the electronic and chemical properties of the specimen.

Deconvolution techniques have therefore been developed to remove the effects of plural scattering from the low-loss spectrum (up to 100 eV) or from ionization edges but very few treatments deal with both angle and energy-loss distributions. Batson & Silcox (1983) have made a detailed study of the inelastic scattering properties of incident 75 keV electrons through a ~100 nm thick polycrystalline aluminium film, over the full range of transferred wavevectors ($0 \rightarrow 3$ Å^{-1}) and energy losses ($0 \rightarrow 100$ eV). Schattschneider (1983) has proposed a matrix approach that is sufficiently elaborate to handle angle-resolved energy-loss data. Simpler deconvolution schemes have been proposed and used for processing multiple losses without specific consideration of angular truncation effects. They are valid when the data have been recorded over sufficiently large angles of collection so that all appreciable inelastic scattering is included. They are generally based on Fourier transform techniques, except for the iterative approach of Daniels, Festenberg, Raether & Zeppenfeld (1970), which has been used for energy losses up to about 60 eV (Colliex, Gasgnier & Trebbia, 1976). The most accurate current methods are the Fourier-log method of Johnson & Spence (1974) and Spence (1979), and the Fourier-ratio method of Swyt & Leapman (1982), which only applies to the core-loss region. The first is far more complete and accurate and applies to any spectral range when one has recorded a full spectrum in unsaturated conditions.

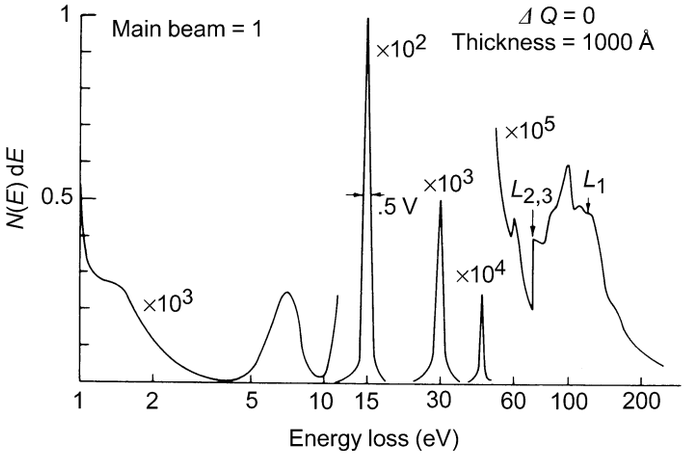

Fig. 4.3.4.3. Excitation spectrum of aluminium from 1 to 250 eV, investigated by EELS on 300 keV primary electrons [courtesy of Schnatterly (1979)].

4.3.4.1.4. *Classification of the different types of excitations contained in an electron energy-loss spectrum*

Figs. 4.3.4.3 and 4.3.4.4 display examples of electron energy-loss spectra over large energy domains, typically from 1 to about 2000 eV. With one instrument, all elementary excitations from the near infrared to the X-ray domain can be investigated. Apart from the main beam or zero-loss peak, two major families of electronic transitions can be distinguished in such spectra:

(*a*) The excitations in the low or moderate energy-loss region ($1 < \Delta E < 50$ eV) concern the quasifree (valence and conduction) electron gas. In a pure metal, such as Al, the dominant feature is the intense narrow peak at 15 eV with its multiple satellites at about 30, 45, and 60 eV. One also detects an interband transition at 1.5 eV and a surface plasmon peak at ~ 7 eV. For the more complex mineral specimen, rhodizite, this contribution lies in the intense and broad, but not very specific, peak around 25 eV. All these features are discussed in detail in Subsection 4.3.4.3.

(*b*) The excitations in the high-energy-loss domain ($50 < \Delta E < 2000$ eV) concern excitation and ionization processes from core atomic orbitals: in Al, the $L_{2,3}$ edge is associated with the creation of holes on the $2p$ level, L_1 is due to the excitation of $2s$, and K of $1s$ electrons. These contributions appear as edges superposed on a regularly decreasing background. In the complex specimen, the succession of these

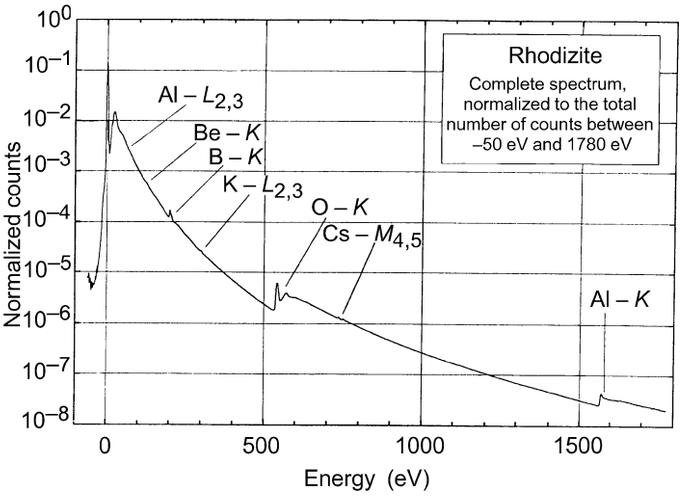

Fig. 4.3.4.4. Complete electron energy-loss spectrum of a thin rhodizite crystal (thickness ~60 nm). Separate spectra from eight significantly overlapping energy ranges were measured and matched. Primary energy 60 keV. Semi-angle of collection 5 mrad. Recording time 300 s (parallel acquisition). Scanned area 30×40 nm. Analysed mass 2×10^{-15} g [courtesy of Engel, Sauer, Zeitler, Brydson, Williams & Thomas (1988)].

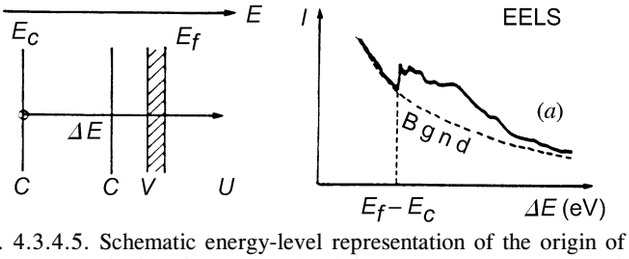

Fig. 4.3.4.5. Schematic energy-level representation of the origin of a core-loss excitation (from a core level C at energy E_c to an unoccupied state U above the Fermi level E_f) and its general shape in EELS, as superimposed on a continuously decreasing background.

references